Science of the Total Environment 663 (2019) 654–661

Contents lists available at ScienceDirect

Science of the Total Environment

journal homepage: www.elsevier.com/locate/scitotenv

Successful control of phosphorus release from sediments using oxygen nano-bubble-modified minerals

Pingping Yu [a,b], Jingfu Wang [a,*], Jingan Chen [a], Jianyang Guo [a], Haiquan Yang [a], Quan Chen [a,c]

[a] State Key Laboratory of Environmental Geochemistry, Institute of Geochemistry, Chinese Academy of Sciences, Guiyang 550081, PR China
[b] College of Resource and Environmental Engineering, Guizhou University, Guiyang 550025, PR China
[c] University of Chinese Academy of Sciences, Beijing 100049, PR China

HIGHLIGHTS

- A specialized aeration material aimed at the sediment-water interface, known as oxygen nano-bubble-modified minerals (ONBMMs) was developed.
- ONBMMs effectively increased the DO at the sediment-water interface.
- ONBMMs remarkably reduced the release flux of sediment P.
- Fe-P precipitation constituted the main mechanism of the inhibition of sediment P release by ONBMMs.

GRAPHICAL ABSTRACT

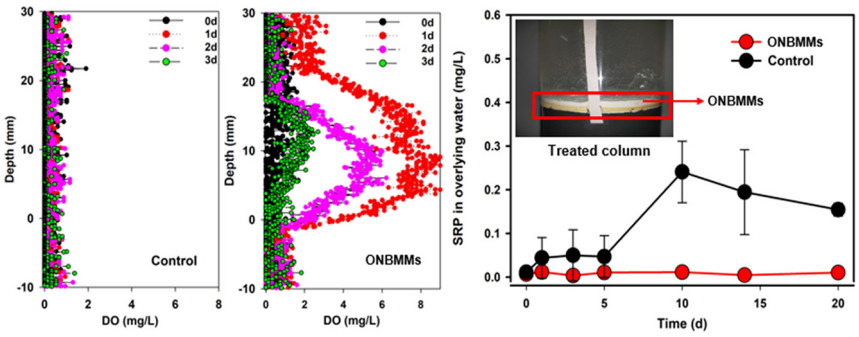

ARTICLE INFO

Article history:
Received 30 November 2018
Received in revised form 14 January 2019
Accepted 19 January 2019
Available online 23 January 2019

Editor: Filip M.G.Tack

Keywords:
Oxygen nano-bubbles-modified minerals
Phosphorus
Sediment-water interface
Diffusive gradients in thin films
Planar luminescent optode technology

ABSTRACT

Due to the limited aeration capacity of current aeration techniques at the sediment-water interface (SWI), we developed a specialized aeration material aimed at the SWI, known as oxygen nano-bubble-modified minerals (ONBMMs). Furthermore, we simulated its aeration efficiency at the SWI and the control effects of internal phosphorous (P) release under anaerobic conditions during 20 days. High resolution diffusive gradients in thin films (DGT) and Planar luminescent optode (PO) technologies were used to measure the temporal variation of reactive P, reactive Fe (II) and dissolved oxygen (DO) of the SWI. These results show that ONBMMs can effectively increase the content of DO at the SWI and decrease the release flux of internal P from sediments. The use of ONBMMs reduced 97.9% of the soluble reactive P concentration of the overlaying water and reduced the release flux of DGT-P from sediments by 78.9%. Inhibition of reductive dissolution of Fe—P from sediments was the primary principle that effectively inhibited the input of internal P by ONBMMs. Therefore, ONBMMs are potentially promising technology for the treatment of internal P pollution in eutrophic lakes.

1. Introduction

Phosphorous (P) is a well-known major limiting factor of lake primary productivity (Carpenter, 2005). The source of P in lakes is mainly categorized as external P, such as industrial wastewater, municipal wastewater and agricultural non-point source pollution, and internal P, which is released from sediments. With the effective controlling of external P, the contribution of internal P to the overall P concentration in lakes continues to increase, reaching 80% in some lakes (Penn et al., 2000; Nausch et al., 2009). As a result, effectively controlling the release of lake internal P is significantly meaningful to resolve lake eutrophication.

* Corresponding author.
E-mail address: wangjingfu@vip.skleg.cn (J. Wang).

https://doi.org/10.1016/j.scitotenv.2019.01.265
0048-9697/

Increasing the dissolved oxygen at the sediment-water interface (SWI) is an important pathway for controlling the release of lake internal P (Wang et al., 2016). Current aeration techniques, such as the artificial delamination technology (Serra et al., 2007), gas lifting technology (Ashley et al., 2008) and bubble plume diffusion technique (McGinnis et al., 2004), all focus on increasing the dissolved oxygen (DO) of the lake bottom with lack of the pertinence to SWI aeration (Conley et al., 2009); therefore, their effects on controlling the release of internal P in lakes are still quite limited (Cowell et al., 1987).

The idea of nano-bubbles (NBs) was first proposed by Parker et al. (Parker et al., 1994). In recent years, the rise of oxygen nano-bubble-modified minerals (ONBMMs) technology provides an opportunity for the development of SWI aeration technologies. Recently, the oxygen nanobubble modified zeolites and local soils were utilized to increase DO and the oxidation-reduction potential (ORP) at the SWI and to change the sediment P from source to sink (Zhang et al., 2018), and used to restore anoxia/hypoxia and control methane emission (Shi et al., 2018). Currently, studies on NBs are relatively limited but it is widely agreed that the formation mechanism of NBs is excess gaseous molecules of the solid-liquid surface that directly nucleate and aggregate on the solid surface in the form of NBs (Zhang et al., 2007). According to the theory of thermodynamics, the existence time of NBs is <1 ms (Lou et al., 2000). However, practical observation indicates that the stability of NBs is far more than the theoretical calculation, as its existence time may vary from several hours to days (Borkent et al., 2007; Ducker, 2009; An et al., 2015). Presently, the long term stable existence of NBs can be explained as follows: 1) the existence of the interface charge on the NB surface is the main reason for the stable existence of the bubble (Ushikubo et al., 2010); 2) there is strong hydrogen bonding in the liquid-vapor interface, which decreases the diffusion and dissolution process of NBs internal gas and prolongs the existence time (Ohgaki et al., 2010); and 3) the internal intensity of the NBs is very high, which could increase their life over 4 magnitudes (Wang et al., 2008). In addition, the mass transfer efficiency of NBs is also significantly higher than that of bubbles in mm/μm that are produced by conventional aeration fashions: 1) the self-supercharging effect of NBs increases the mass transfer efficiency of the liquid-vapor interface (Wang et al., 2008); and 2) the huge surface energy of the NBs can greatly increase the utilization efficiency of oxygen on the bubble surface (Tasaki et al., 2009).

Because of prominent advantages, such as a long stable time and high mass transfer efficiency (Tyrrell and Attard, 2001; Shi et al., 2018; Fang et al., 2018), NBs have a vast application potential from the perspective of lake SWI aeration and internal P control (Zhang et al., 2018). This study utilized a natural mineral (muscovite) as a base for the loading of oxygen nano-bubbles to develop a specialized novel material and technique for aeration of the SWI. In this study, diffusive gradients in thin films (DGT) and Planar luminescent optode (PO) technologies were applied in a simulation experiment for aeration of ONBMMs in order to control internal P release under anaerobic conditions. The objectives of this study were to: 1) quantify the aeration efficiency of ONBMMs at the SWI and the controlling effects of internal P release; and 2) investigate the effects of ONBMMs treatment on P (Fe) distribution at the SWI and elucidate the possible mechanism for controlling the release of P from sediments.

2. Materials and methods

2.1. Preparation of ONBMMs

Nano-bubbles were prepared using the methanol-water replacement method (Hampton et al., 2008; Karpitschka et al., 2012). Briefly, pure oxygen with a flux of 300 mL/min was aerated into methanol (purity >99.9%) with the saturated methanol solution being obtained after aeration for 30 min at 20 °C. The obtained solution was then placed into a beaker and 100 g of muscovite mineral particles was added for invasion. The excess methanol was removed after standing for 10 min. Ultrapure water was used to replace methanol (V_1:V_2 = 9:1, where V_1 denotes the volume of ultrapure water and V_2 denotes the volume of methanol), and then the oxygen nano-bubbles formed on the surface of the mineral due to over saturation.

2.2. Simulation experiment and sampling

Six parallel samples of sediment column cores were collected using a gravity sampler from the Hongfeng Reservoir (26°30′N, 106°23′E), which is a reservoir with deep water eutrophication located in southwestern China. After collecting the column cores, they were sealed with rubber plugs, encapsulated with silver paper to avoid light and transported to the lab within 2 h. The total height of the sediment column cores was 50 cm, with inner diameter of 11 cm, and the mud-water height ratio was approximately 2:3. In addition, the lake water samples (20 L) was collected from the bottom for chemical analysis and simulation experiments.

Two experimental groups were conducted, namely "with" (Core a, b and c) and "without" (Core d, e and f) the addition of ONBMMs, with three replicates in each group. The overlaying water was controlled under anaerobic conditions (DO < 1 mg/L) by continuous pumping of an adequate amount of pure N_2. The incubation temperature was set as 20 °C ± 1 °C. These environmental conditions were consistent with that of the bottom water in the Hongfeng Reservoir. The cycle of the simulation experiment was 20 days.

On days 0, 1, 3, 5, 14 and 20, 20 mL samples were collected from the overlaying water. After each sampling, the same volume of bottom water was supplemented. In future calculations, these volumes were corrected for. On days 0, 1, 5, 14 and 20, the ZrO-Chelex DGT (Easysensor Ltd., Nanjing, China) was plugged at the SWI of the column core and recycled after standing for 24 h.

2.3. Chemical analysis

The total P (TP) and soluble reactive P (SRP) in the overlaying water samples were measured using the molybdenum-blue method (Murphy and Riley, 1962). After recycling the ZrO-Chelex DGT probes, the gel surface of the ZrO-Chelex was washed with deionized water and the samples were cut with an interval of 2 mm and then placed into 1.5 mL centrifuge tubes. The reactive Fe (II) (DGT-Fe) and reactive P (DGT-P) were extracted using 1 mol/L nitric acid and 1 mol/L sodium hydroxide from the DGT samples after cutting (Ding et al., 2015; Ren et al., 2018). The DGT-Fe concentrations of the extracts were measured by Ferroin colorimetry (Tamura et al., 1974). The DGT-P concentration in the extract was measured using Epoch Microplate Spectrophotometry (Epoch Microplate Spectrophotometer, Biotek, USA) (Ding et al., 2012; Jin et al., 2019).

On days 0, 1, 2, 3, the distribution of DO around the SWI was measured using the PO technology (VisiSens TD, PreSens Precision Sensing GmbH, Germany). It should be noted that the plane electrode films needed to be cut into 1 cm × 10 cm pieces and pasted on the inner wall of the upper part of the plexiglass sampling tube before sediment column core collection. This plane electrode film was long enough to ensure the position of the SWI was covered within the length range.

2.4. The release flux of P from the sediment-water interface

To quantify the inhibition capacity of ONBMMs to the release of P from sediments, the input flux of internal P in the sediment column cores of groups with and without the addition of ONBMMs were both calculated. The calculation utilized two methods, namely the method based on the variation of the P concentration in the overlaying water over time and the method based on the high-resolution concentration gradient of P around the SWI.

Firstly, the release speed of P ($mg/m^2/d$) from the sediment was calculated using the variation of the P concentration in the sediment

column core over time as follows (Eq. 1; Fisher and Reddy, 2001; Ding et al., 2015):

$$F = \left[V(C_n - C_0) + \sum_{j=1}^{n} V_{j-1}(C_{j-1} - C_a)\right]/(A \times t) \quad (1)$$

In which, V denotes the volume of the overlaying water (L) of the bottom sludge column; V_{j-1} denotes the volume (L) of the water sample taken at j-1 time; C_0, C_n and C_{j-1} denote the P concentration (mg/L) of the water sample taken at 1, n and j-1 time, respectively; C_a denotes the P concentration (mg/L) in the supplement water; A denotes the surface area (m^2) of sediments; and t denotes time (d).

Secondly, in the unstable diffusion process of the sediment, the variation rate of the P concentration over time equaled the negative value of the variation rate of the diffusion flux with distance (Lavery et al., 2001). According to Fick's first law, the release flux of P through the SWI can be expressed as follows (Eq. 2; Ullman and Aller, 1982; Yu et al., 2017; Lin et al., 2019):

$$F = \phi \times D_s \frac{\partial C}{\partial Z}\Big|_{z=0} \quad (2)$$

In which, F denotes the release flux ($mg/m^2/d$); ϕ denotes the porosity of surface sediments, and It has a value between 0.92 and 0.96; D_S denotes the effective diffusion coefficient of ion in sediments (Li and Gregory, 1974). The Ds value can be calculated as follows (Yu et al., 2017):

$$D_s = \phi D_0, \phi < 0.7 \quad (3)$$

$$D_s = \phi^2 D_0, \phi > 0.7 \quad (4)$$

where D_0 is the ideal diffusion coefficient of the infinite dilution solution. The D_0 value used in this study was 7.34×10^{-6} cm^2/s (Yu et al., 2017), so D_S was estimated between 6.21×10^{-6} cm^2/s and 6.76×10^{-6} cm^2/s. $\frac{\partial C}{\partial Z}$ denotes the concentration gradient with linear variation of P around the SWI, which was usually within a spatial range of several tens of mm above or below the SWI.

2.5. Statistical analysis

The data used in this study was plotted using Origin 2017 (Origin Lab Inc., USA) and SigmaPolt 10.0 (Systat Software Inc., USA). Pearson correlation analysis was used to test the correlation between the DGT-P and DGT-Fe of sediments in the groups with and without addition of ONBMMs and the control group. This study utilized SPSS 13.0 (IBM Corp., USA) for statistical analysis.

3. Results

3.1. The effects of ONBMMs on the DO distribution at the SWI

The temporal variation of DO around the SWI of the sediment column core with different treatments is shown in Fig. 1. After adding ONBMMs for one day, there was an obvious DO peak at the 1–2 cm range around the SWI of the column cores with the addition of ONBMMs (Fig. 1a–c). Due to the error of experimental operation, the results from a, b and c had some gaps. The maximum DO in column core c was over 9 mg/L and the thickness of the aerobic regions was 25 mm. The aerobic region around the SWI of column core a was the thinnest (13 mm) and the maximum DO was 6.2 mg/L. The thickness of the aerobic region around the SWI of column core b was between that of a and c, the maximum DO was 6.5 mg/L. In the control group without the addition of ONBMMs, the region around the SWI in the three column cores had no obvious DO concentration peak and the mean was <1 mg/L, indicating that no aerobic regions were created around the SWI (Fig. 1d–f).

For the three column cores in the group with the addition of ONBMMs, as time progressed, both the DO concentration around the SWI and the thickness of the aerobic region gradually decreased (Fig. 1a–c). After 3 days, the DO concentration peak around the SWI gradually disappeared and <2 mg/L. For the three column cores in the control group without the addition of ONBMMs, the DO concentration around the SWI did not increase or decrease with time, remaining at a low concentration and about 1 mg/L (Fig. 1d–f).

3.2. The effects of ONBMMs on the concentration of TP and SRP in overlaying water

The variation of TP and SRP concentrations over time in the overlaying water of sediment column cores with different treatments is shown in Fig. 2. For column cores of the control group, the average concentration of TP and SRP in the overlaying water continuously increased from 0.04 ± 0.01 mg/L to 0.42 ± 0.16 mg/L and from 0.01 ± 0.00 mg/L to 0.15 ± 0.02 mg/L, respectively. For column cores with addition of ONBMMs, the average concentrations of TP and SRP in the overlaying water were both obviously lower than that of control group. Specifically, the average concentration of TP in the overlaying water slightly increased from 0.05 ± 0.01 mg/L to 0.09 ± 0.02 mg/L while the average concentration of SRP in the overlaying water remained at a low level (0.01 ± 0.00 mg/L).

3.3. The effects of ONBMMs on the distribution of DGT-P and DGT-Fe at the SWI

The variation of DGT-P and DGT-Fe concentrations over time in sediment column cores with different treatments is shown in Figs.3 and 4, respectively. For the three sediment column cores with the addition of ONBMMs, the DGT-P concentration of the sediment gradually decreased over time (Fig. 3a–c), maximum drop from 4 mg/L to 0.2 mg/L. In particular, the concentration gradient of DGT-P was obviously reduced from 0 to 15 mm below the SWI, indicating that the release of reactive P from the sediment was obviously inhibited. This decrease of the DGT-P concentration gradient became very obvious after ONBMMs were added for one day, showing that the inhibition speed of the reactive P release from sediments was very fast. After 14 days, the concentration gradient of DGT-P completely disappeared from 0 to 30 mm below the SWI of column core c (Fig. 3c). For the three column cores in the control group, the concentration of DGT-P slightly decreased (from 4 mg/L to 2 mg/L) over time in the sediment but this trend was not obvious (Fig. 3d–f). An obvious concentration gradient of DGT-P still existed from 0 to 20 mm below the SWI of the three column cores.

For the three sediment column cores with the addition of ONBMMs, the concentration variations of DGT-Fe over time at the SWI were similar to that of DGT-P (Fig. 4a–c). As time progressed, the concentration of DGT-Fe gradually decreased in the sediments and maximum drop from 15 mg/L to 0.1 mg/L. In particular, from 0 to 10 mm below the SWI, the concentration gradient of DGT-Fe obviously decreased. After 14 days, the concentration gradients of DGT-Fe around the SWI of column cores a and c completely disappeared (Fig. 4a, c). For the three sediment column cores of the control group, the concentration gradients of DGT-Fe in the sediment also showed a decreasing trend as time increased, especially after 14 days (Fig. 4d–f). Nevertheless, an obvious concentration gradient of DGT-Fe could still be observed around the SWI of these three column cores, and the concentration was >2 mg/L at 10 mm below the SWI.

3.4. The effects of ONBMMs on the release flux of internal P

The release flux of internal P in the sediment column cores with different treatments is shown in Table 1. Firstly, the release flux of P from sediments (F_1) was calculated based on the temporal variation of the SRP concentration in the overlaying water of the column cores. For the three column cores with the addition of ONBMMs, the release flux of P

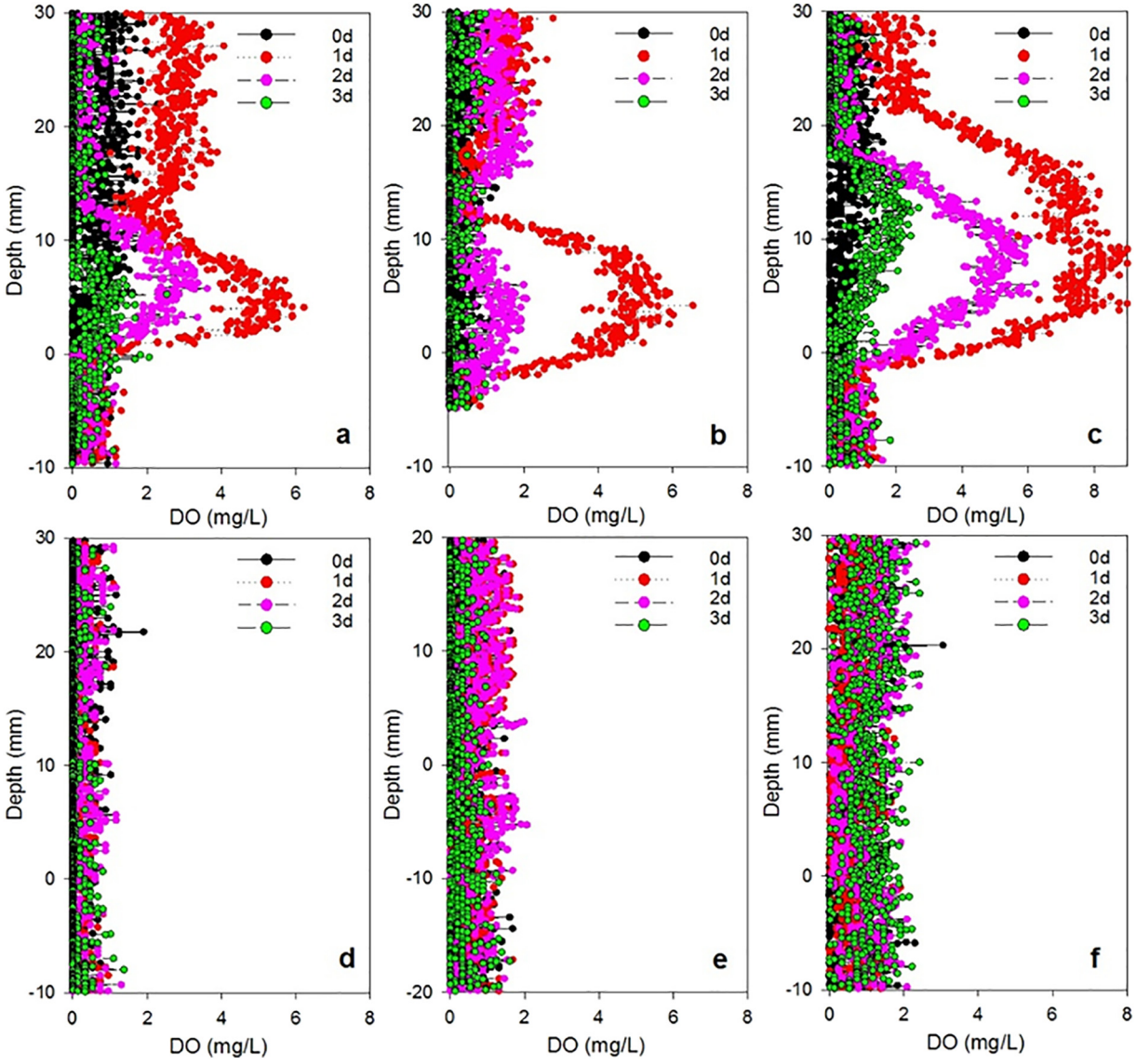

Fig. 1. Variation of dissolved oxygen concentration with time at sediment-water interface in cores treated (a, b, c) and untreated (d, e, f) with ONBMMs.

from the sediments (F_1) was 0.002, 0.05 and 0.10 mg/m^2/d, respectively (mean: 0.05 mg/m^2/d). For column cores of the control group, the release flux of P from sediments (F_1) ranged from 2.09 to 2.49 mg/m^2/d (mean: 2.33 mg/m^2/d). Secondly, the release flux of P from sediments (F_2) was calculated based on the concentration gradient of soluble P at the SWI and Fick's first law. The release flux of P from the sediment

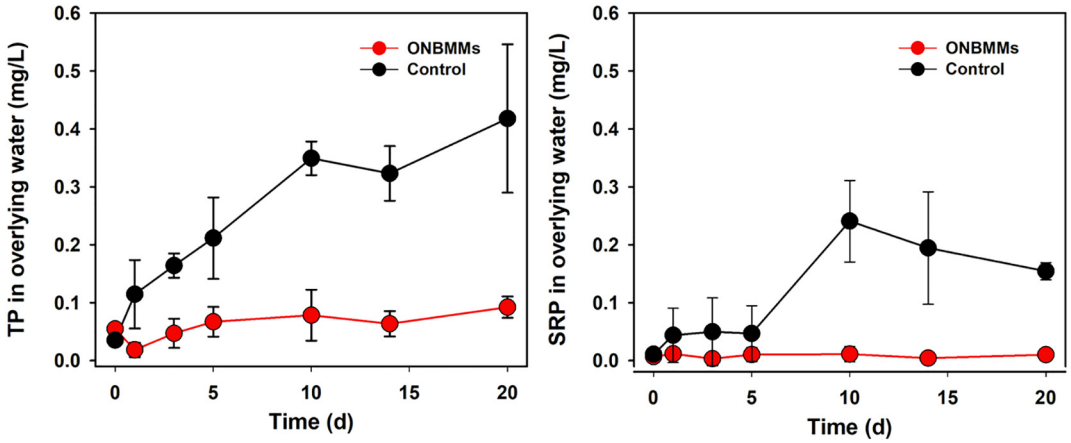

Fig. 2. Variation of TP and SRP concentration in overlying water of sediment cores treated and untreated with ONBMMs.

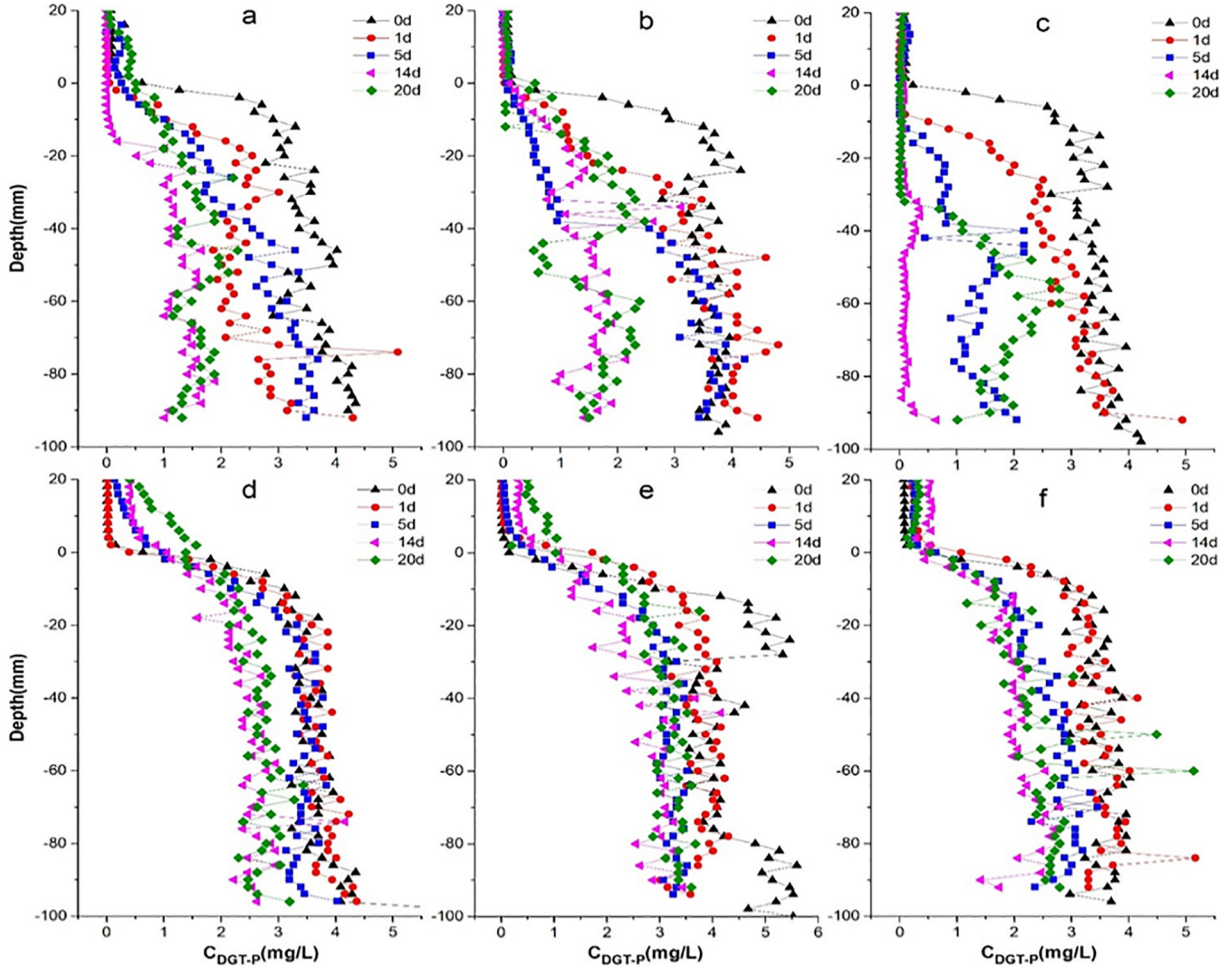

Fig. 3. Variation of DGT-P concentration with time and depth at the sediment-water interface in cores treated (a, b, c) and untreated (d, e, f) with ONBMMs.

column cores with the addition of ONBMMs (F_2) was 2.07, 2.42 and 0.18 mg/m^2/d, respectively (mean: 1.56 mg/m^2/d) and that of the control group was 5.71, 9.21 and 7.25 mg/m^2/d respectively (mean: 7.39 mg/m^2/d). Although the calculated results of the two methods were different, they both indicate that ONBMMs effectively inhibit the release of P from sediments.

Since the oxygen loading of ONBMMs was not accurately controlled in the parallel samples (sediment column cores), the degree of variation for the release flux of P from sediments in the group with the addition of ONBMMs was relatively large, thus the release flux of P from sediments in groups with and without the addition of ONBMMs were estimated. From the perspective of the SRP concentration variation in overlaying water of the column cores, the release flux of internal P was reduced from 2.33 mg/m^2/d without the addition of ONBMMs to 0.05 mg/m^2/d with the addition of ONBMMs, which is a reduction of 97.9%. For the perspective of the DGT-P concentration gradient at the SWI, the release flux of internal P was also reduced from 7.39 mg/m^2/d to 1.56 mg/m^2/d without the addition of ONBMMs, which is a reduction of 78.9%. These quantitative results reveal that ONBMMs effectively decreased the input of internal P in the sediment column cores.

4. Discussion

4.1. The mechanism by which ONBMMs reduce the release of internal P

Pearson correlation analysis demonstrates that DGT-P and DGT-Fe concentrations in sediments from the Hongfeng Reservoir have a significant positive correlation ($r^2 > 0.90$, $p < 0.01$; Fig. 5). This indicates that reactive P and reactive Fe (II) are synchronously released from the sediment, thereby supporting the point that the release of P from sediments is controlled by reductive dissolution of iron bound P (Ding et al., 2016; Ding et al., 2018; Chen et al., 2018). Therefore, the release of P from sediments in the Hongfeng Reservoir is controlled by oxidation and reduction conditions at the SWI. Under aerobic conditions, a thin aerobic layer would be formed, where Fe mainly exists in the form of oxides (Froelich et al., 1979). The relatively large specific surface area and strong ion adsorption ability of Fe oxides could prevent desorption and release of reactive P from the sediments (Nóbrega et al., 2014). In contrary, when the SWI is under anaerobic conditions, Fe^{3+} in the surface sediments is reduced to Fe^{2+} with the reductive dissolution of Fe—P in the sediments. Therefore, P is strongly released from sediments under anaerobic conditions.

The Fe content of surface sediments in the Hongfeng Reservoir was very high, which was the main form of P in sediments (272 mg/kg, average; Wang et al., 2016). During the anaerobic period in the summer, the reductive dissolution of Fe—P in the sediments forms a large amount of SRP, which passes the SWI and leads to the strong release of internal P from the sediments. This is consistent with the variation of SRP and TP concentrations in the overlaying water of the simulation experiment (Fig. 2). After adding ONBMMs, the oxygen continuously released by the ONBMMs made the SWI aerobic, forming a passivation layer of Fe oxides, which locked the reactive P (SRP/DGT-P) strictly in the sediment, thus effectively reducing the release of internal P (Table1). Under anaerobic conditions and without the addition of ONBMMs, DGT-P had a very high concentration gradient at the SWI (Fig. 3), leading to a strong release of internal P from the sediment.

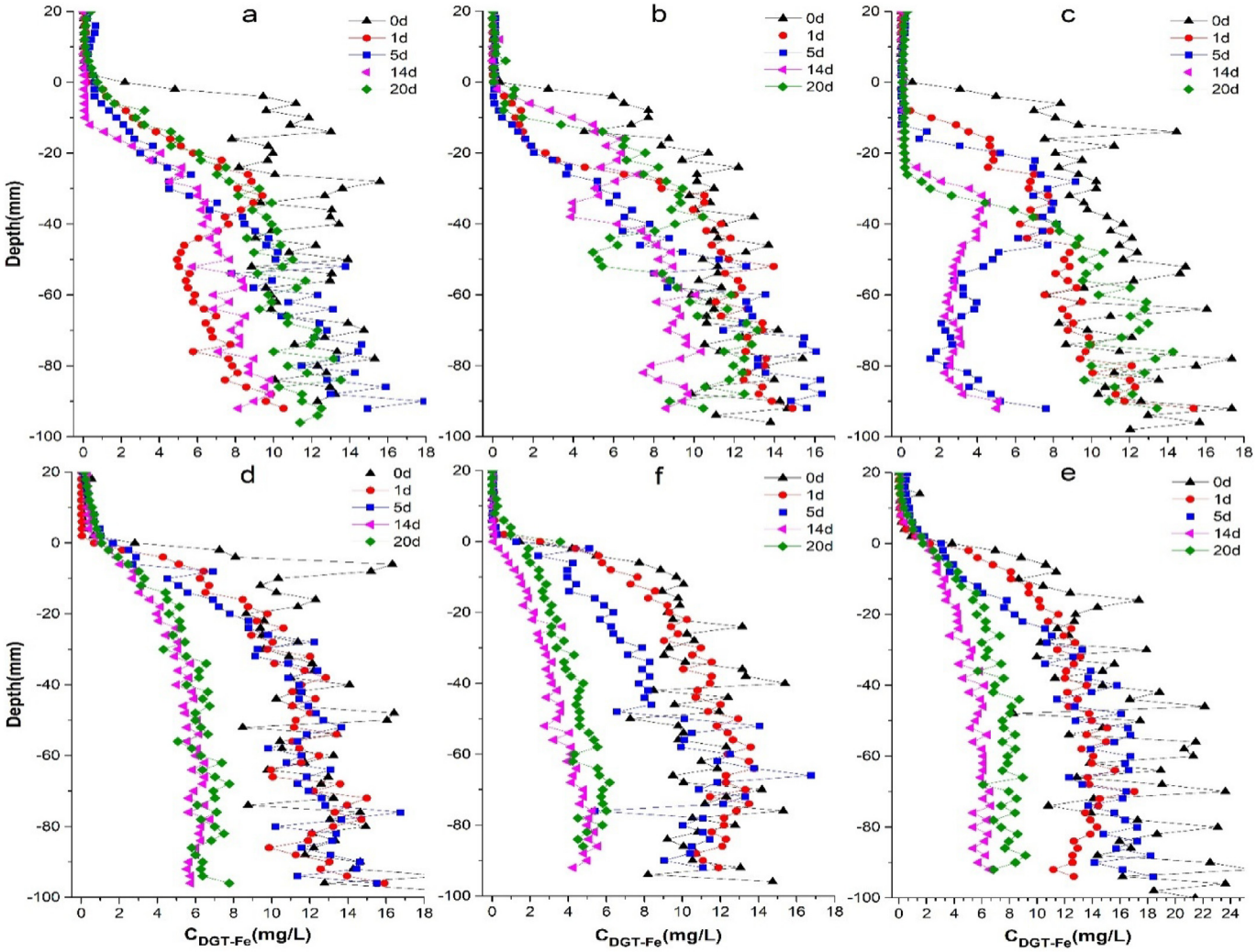

Fig. 4. Variation of DGT-Fe concentration with time and depth at the sediment-water interface in cores treated (a, b, c) and untreated (d, e, f) with ONBMMs.

However, when ONBMMs were added on the sediment surface, the oxygen continuously released by the NBs of the ONBMMs formed an oxidation layer at the SWI, which not only decreased the concentrations of DGT-P and DGT-Fe, but also greatly reduced the concentration gradient of DGT-P at the SWI, thus inhibiting the release of internal P from the sediments. The NBs of the ONBMMs also played a significant role here.

4.2. Practical application of ONBMMs

Nano-bubble studies are still in the preliminary stage (Parker et al., 1994; Zhang et al., 2007). The application of NBs for the treatment of water pollution in lakes (reservoirs) is an exploratory mission (Pan et al., 2016). In this study, the developed ONBMMs material has unique advantages for the aeration of the lake SWI, such as strong pertinence, low cost, convenient operation and quick effectiveness. Compared with other control technologies, such as in-situ P immobilization using P-sorbents, ONBMMs has the advantages of low ecological risk, low-cost and simple operation, our results are equally considerable. Aluminum-modified clay, zirconium-reacted bentonite (ZrBT) and a P-capping agent-700 °C-heated natural calcium-rich attapulgite (NCAP700) was utilized to study the influence of on the release flux of P in sediments and concluded that under anaerobic condition, aluminum-modified clay reduced the release flux of P by 95.9% (Wang et al., 2019), most of PO_4^{3-} bound by ZrBT (about 87% of bound PO_4^{3-}) (Lin et al., 2016), the P flux in overlying water and pore water of sediments was both inhibited, and 34.5% of P_{mobile} was bound in the upper 2 cm sediment layer by NCAP700 (Yin and Kong, 2015). However, not all P release from sediments could be controlled by oxygenation technology. For example, P release from sediments in Lake Dianchi, SW China, is controlled by pH and microbial action. ONBMMs technique is not applicable in such cases. In addition, there are still essential issues that needed to be solved before ONBMMs technology is applied for in-field engineering. Firstly, the timeliness of ONBMMs needs to be further quantified. The stable existence time of NBs remains a big challenge because the stability mechanism of NBs is unclear (Ishida et al., 2000; Zhang et al., 2007; Seddon et al., 2011; Pan et al., 2016). Previous studies report that the NB can slowly oxygenate water last >70 days when diameter is <200 nm (Zhang et al., 2018). However, there is still a gap between this period and the seasonal

Table 1
Sediment P release flux in sediment cores treated and untreated with ONBMMs.

Sediment P release flux ($mg/m^2/d$)	Treated with ONBMMs			Untreated with ONBMMs		
	a	b	c	d	e	f
F_1[a]	0.002	0.05	0.10	2.49	2.40	2.09
F_2[b]	2.07	2.42	0.18	5.71	9.21	7.25

[a] Flux calculated based on the variations in the P concentration of overlying water over time.
[b] Flux calculated based on the P concentration gradient at the SWI and Fick's first law.

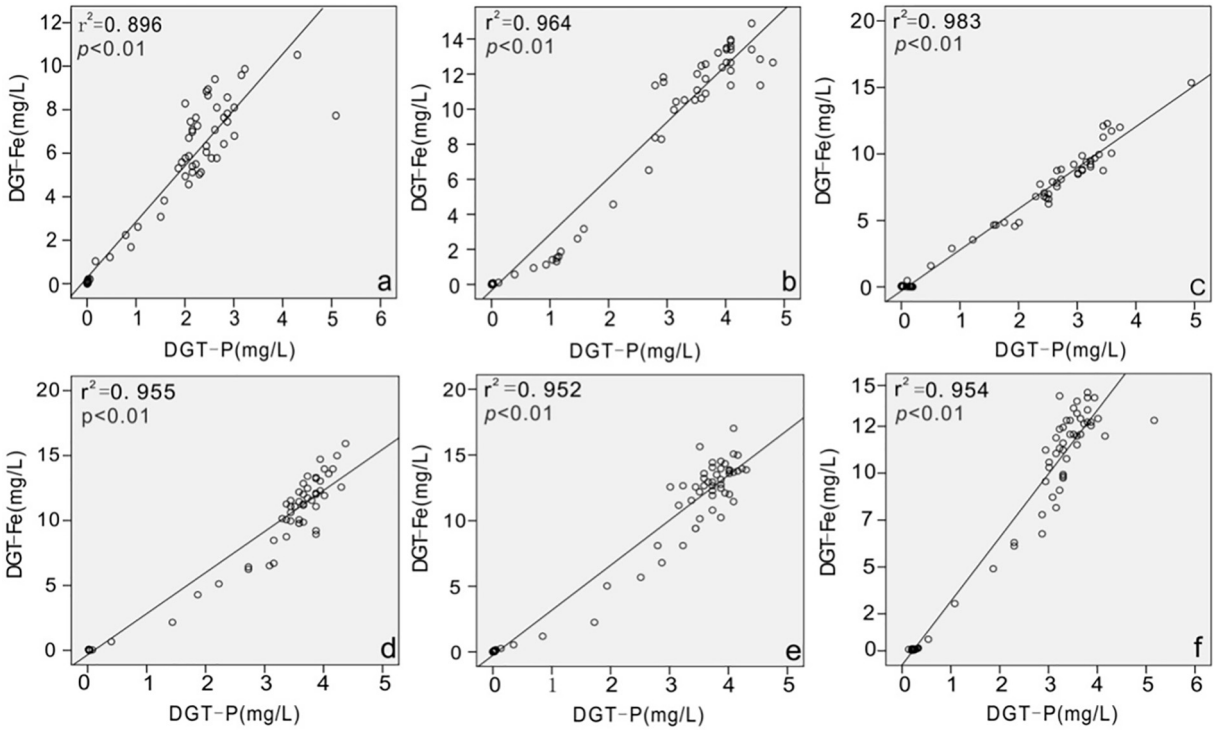

Fig. 5. Correlation between DGT-P and DGT-Fe concentration in parallel sediment profiles treated (a, b, c) and untreated (d, e, f) with ONBMMs.

anaerobic time of natural water bodies (lakes/reservoirs) and multiple additions might be an option to solve this issue. Secondly, the gas loading volume of ONBMMs, which is determined the aeration capacity of the ONBMMs, needs to be further improved. The higher the gas loading volume, the more oxygen that is provided by the ONBMMs for the SWI, which could be more favorable for controlling the pollution of internal P. Using methods such as mineral screening and hydrophobic modification to improve the gas loading volume is an important direction for future studies. Thirdly, the field addition issue of ONBMMs is still not completely solved. ONBMMs material is a mixture of solids and liquids, because NBs exist at the interface of solids and liquids (Parker et al., 1994; Ishida et al., 2000; Zhang et al., 2007). When the treated water body is relatively deep, it becomes an important technique to settle ONBMMs at the SWI in time without a large loss of NBs. This requires the development of matching equipment. Finally, the disturbance rejection capacity of ONBMMs needs to be further estimated. In water bodies with strong hydrodynamic forces, disturbances may cause the abscission of bubbles on the surface of ONBMMs and reduce the effects of aeration. In all, ONBMMs technology has unique advantages but some issues still need further study before engineering application.

5. Conclusion

In this study, a specialized aeration material, ONBMMs, aimed at the lake SWI was developed. Their aeration efficiency at the SWI and the controlling effects of internal P release were tested under anaerobic conditions. The use of ONBMMs enabled the DO in the region of 10–20 mm around the SWI to reach over 6 mL/L, which had obvious and quick aeration effects on the SWI. ONBMMs changed the oxidation and reduction conditions of the surface sediments, which could effectively inhibit the release of P from the sediments to the overlaying water. The aeration of ONBMMs to the SWI had some advantages, such as high efficiency, quick effectiveness, low cost and convenient operation; thus, this technology has great potential for aeration of the SWI and internal pollution treatment in lakes (reservoirs).

Acknowledgements

This study was sponsored jointly by CAS Interdisciplinary Innovation Team, the Chinese NSF project (No. 41773145), the National Key Research and Development Project by MOST of China (No. 2016YFA0601000), the Youth Innovation Promotion Association CAS, and the Department of Science and Technology of Guizhou Province ([2015]2001 and [2016]2802).

References

An, H.J., Liu, G.M., Atkin, R., Craig, V.S.J., 2015. Surface nanobubbles in nonaqueous media: looking for nanobubbles in DMSO, formamide, propylene carbonate, ethylammonium nitrate, and propylammonium nitrate. ACS Nano 9 (7), 7596–7607.

Ashley, K.I., Mavinic, D.S., Hall, K.J., 2008. Oxygenation performance of a laboratory-scale Speece Cone hypolimnetic aerator: preliminary assessment. Can. J. Civ. Eng. 35 (7), 663–675.

Borkent, B.M., Dammer, S.M., Holger, S., Vancso, G.J., Lohse, D., 2007. Super stability of surface nanobubbles. Phys. Rev. Lett. 98 (20), 204502.

Carpenter, S.R., 2005. Eutrophication of aquatic ecosystems: Bistability and soil P. PNAS 102, 10002–10005.

Chen, M.S., Ding, S.M., Chen, X., Sun, Q., Fan, X.F., Lin, J., et al., 2018. Mechanisms driving phosphorus release during algal blooms based on hourly changes in iron and phosphorus concentrations in sediments. Water Res. 133, 153–164.

Conley, D.J., Bonsdorff, E., Carstensen, J., Destouni, G., Gustafsson, B.G., Hansson, L.A., et al., 2009. Tackling hypoxia in the Baltic Sea: is engineering a solution? Environ. Sci. Technol. 43 (10), 3407–3411.

Cowell, B.C., Dawes, C.J., Gardiner, W.E., Scheda, S.A., 1987. The influence of whole lake aeration on the limnology of a hypereutrophic lake in central Florida. Hydrobiologia 148, 3–24.

Ding, S.M., Sun, Q., Xu, D., Jia, F., He, X., Zhang, C., 2012. High-resolution simultaneous measurements of dissolved reactive phosphorus and dissolved sulfide: the first observation of their simultaneous release in the sediments. Environ. Sci. Technol. 46 (15), 8297–8304.

Ding, S.M., Han, C., Wang, Y.P., Yao, L., Wang, Y., Xu, D., et al., 2015. In situ, high-resolution imaging of labile phosphorus in sediments of a large eutrophic lake. Water Res. 74, 100–109.

Ding, S.M., Wang, Y., Wang, D., Li, Y.Y., Gong, M.D., Zhang, C.S., 2016. In situ, high-resolution evidence for iron-coupled mobilization of phosphorus in sediments. Sci. Rep. 6, 24341.

Ding, S.M., Chen, M.S., Gong, M.D., Fan, X.F., Qin, B.Q., Xu, H., et al., 2018. Internal phosphorus loading from sediments causes seasonal nitrogen limitation for harmful algal blooms. Sci. Total Environ. 625, 872–884.

Ducker, W.A., 2009. Contact angle and stability of interfacial nanobubbles. Langmuir 25 (16), 8907–8910.

Fang, Z., Wang, Lei., Wang, X.Y., Zhou, L.M., Wang, S., Zou, Z.L., et al., 2018. Formation and stability of surface/bulk nanobubbles produced by decompression at lower gas concentration. J. Phys. Chem. C 122, 22418−−22423.
Fisher, M.M., Reddy, K.R., 2001. Phosphorus flux from wetland soils affected by long term nutrient loading. J. Environ. Qual. 30, 261–271.
Froelich, P.N., Klinkhammer, G.P., Bender, M.L., Luedtke, N.A., Heath, G.R., Cullen, D., et al., 1979. Early oxidation of organic matter in pelagic sediments of the eastern equatorial Atlantic: suboxic diagenesis. Geochim. Cosmochim. Acta 43 (7), 1075–1090.
Hampton, M.A., Donose, B.C., Nguyen, A.V., 2008. Effect of alcohol-water exchange and surface scanning on nanobubbles and the attraction between hydrophobic surfaces. J. Colloid Interface Sci. 325 (1), 267–274.
Ishida, N., Inoue, T., Miyahara, M., Higashitani, K., 2000. Nanobubbles on a hydrophobic surface in water observed by tapping-mode atomic force microscopy. Langmuir 16 (16), 6377–6380.
Jin, Z.F., Ding, S.M., Sun, Q., Gao, S.S., Fu, Z., Gong, M.D., et al., 2019. High resolution spatiotemporal sampling as a tool for comprehensive assessment of zinc mobility and pollution in sediments of a eutrophic lake. J. Hazard. Mater. 364, 182–191.
Karpitschka, S., Dietrich, E., Seddon, J.R.T., Zandvliet, H.J.W., Lohse, D., Riegler, H., 2012. Nonintrusive optical visualization of surface nanobubbles. Phys. Rev. Lett. 109 (6), 066102.
Lavery, P.S., Oldham, C.E., Ghisalberti, M., 2001. The use of Fick's first law for predicting porewater nutrient fluxes under diffusive conditions. Hydrol. Process. 15 (13), 2435–2451.
Li, Y.H., Gregory, S., 1974. Diffusion of ions in sea-water and in deep-sea sediments. Geochim. Cosmochim. Acta 38, 703–714.
Lin, J.W., Wang, H., Zhan, Y.H., Zhang, Z., 2016. Evaluation of sediment amendment with zirconium-reacted bentonite to control phosphorus release. Environ. Earth Sci. 75 (11), 942–958.
Lin, J.W., He, S.Q., Zhang, H.H., Zhan, Y.H., Zhang, Z.B., 2019. Effect of zirconium-modified zeolite addition on phosphorus mobilization in sediments. Sci. Total Environ. 646, 144–157.
Lou, S.T., Ouyang, Z.Q., Zhang, Y., Li, X.J., Hu, J., Li, M.Q., 2000. Nanobubbles on solid surface imaged by atomic force microscopy. J. Vac. Sci. Technol. B 18 (5), 2573–2575.
McGinnis, D.F., Lorke, A., Wuest, A., Stöckli, A., Little, J.C., 2004. Interaction between a bubble plume and the near field in a stratified lake. Water Resour. Res. 40 (10), 11–21.
Murphy, J., Riley, J.P., 1962. A modified single solution method for the determination of phosphate in natural waters. Anal. Chim. Acta 27, 31–36.
Nausch, M., Nausch, G., Lass, H.U., Mohrholz, V., Nagel, K., Siegel, H., et al., 2009. Phosphorus input by upwelling in the Eastern Gotland Basin (Baltic Sea) in summer and its effects on filamentous cyanobacteria. Estuar. Coast. Shelf Sci. 83 (4), 434–442.
Nóbrega, G.N., Otero, X.L., Macias, F., Ferreira, T.O., 2014. Phosphorus geochemistry in a Brazilian semiarid mangrove soil affected by shrimp farm effluents. Environ. Monit. Assess. 186, 5749–5762.
Ohgaki, K., Khanh, N.Q., Joden, Y., Tsuji, A., Nakagaw, T., 2010. Physicochemical approach to nanobubble solutions. Chem. Eng. Sci. 65 (3), 1296–1300.
Pan, G., He, G.Z., Zhang, M.Y., Zhou, Q., Tyliszczak, T., Tai, R.Z., 2016. Nanobubbles at hydrophilic particle−water interfaces. Langmuir 32 (43), 11133–11137.
Parker, J.L., Claesson, P.M., Attard, P., 1994. Bubbles, cavities, and the long-ranged attraction between hydrophobic surfaces. J. Phys. Chem. 98 (34), 8468–8480.
Penn, M.R., Auer, M.T., Doerr, S.M., Driscoll, C.T., Brooks, C.M., Effler, S.W., 2000. Seasonality in phosphorus release rates from the sediments of a hypereutrophic lake under a matrix of pH and redox conditions. Can. J. Fish. Aquat. Sci. 57 (5), 1033–1041.
Ren, M.Y., Ding, S.M., Fu, Z., Yan, L.Y., Tang, W.Y., Tsang, D.C.W., et al., 2018. Seasonal antimony pollution caused by high mobility of antimony in sediments: in situ evidence and mechanical interpretation. J. Hazard. Mater. 367, 427–436.
Seddon, J.R.T., Zandvliet, H.J.W., Lohse, D., 2011. Knudsen gas provides nanobubble stability. Phys. Rev. Lett. 107 (9), 116101.
Serra, T., Vidal, J., Casamitjana, X., Soler, M., Colomer, J., 2007. The role of surface vertical mixing in phytoplankton distribution in a stratified reservoir. Limnol. Oceanogr. 52, 620–634.
Shi, W.Q., Pan, G., Chen, Q.W., Song, L.R., Zhu, L., Ji, X.N., 2018. Hypoxia remediation and methane emission manipulation using surface oxygen nanobubbles. Environ. Sci. Technol. 52 (15), 8712–8717.
Tamura, H., Goto, K., Yotsuyanagi, T., Nagayama, M., 1974. Spectrophotometric determination of iron(III) with 1, 10-phenanthroline in the presence of large amounts of iron(III). Talanta 21, 314–318.
Tasaki, T., Wada, T., Baba, Y., Kukizaki, M., 2009. Degradation of surfactants by an integrated nanobubbles/VUV irradiation technique. Ind. Eng. Chem. Res. 48 (9), 4237–4244.
Tyrrell, J.W.G., Attard, P., 2001. Images of nanobubbles on hydrophobic surfaces and their interactions. Phys. Rev. Lett. 87, 176104.
Ullman, W.J., Aller, R.C., 1982. Diffusion coefficients in nearshore marine sediments. Limnol. Oceanogr. 27, 552–556.
Ushikubo, F.Y., Furukawa, T., Nakagawa, R., Enari, M., Makino, Y., Kawagoe, Y., 2010. Evidence of the existence and the stability of nano-bubbles in water. Colloids Surf. A Physicochem. Eng. Asp. 361 (1), 31–37.
Wang, S.R., Jin, X.C., Bu, Q.Y., Jiao, L.X., Wu, F.C., 2008. Effects of dissolved oxygen supply level on phosphorus release from lake sediments. Colloids Surf. A Physicochem. Eng. Asp. 316 (1–3), 245–252.
Wang, J.F., Chen, J.A., Ding, S.M., Guo, J.Y., Christopher, D., Dai, Z.H., et al., 2016. Effects of seasonal hypoxia on the release of phosphorus from sediments in deep-water ecosystem: a case study in Hongfeng Reservoir, southwest China. Environ. Pollut. 219, 858–865.
Wang, J.F., Chen, J.A., Chen, Q., Yang, H.Q., Zeng, Y., Yu, P.P., et al., 2019. Assessment on the effects of aluminum-modified clay in inactivating internal phosphorus in deep eutrophic reservoirs. Chemosphere 215, 657–667.
Yin, H.B., Kong, M., 2015. Reduction of sediment internal P-loading from eutrophic lakes using thermally modified calcium-rich attapulgite-based thin-layer cap. J. Environ. Manag. 151, 178–185.
Yu, J.H., Ding, S.M., Zhong, J.C., Fan, C.X., Chen, Q.W., Yin, H.B., et al., 2017. Evaluation of simulated dredging to control internal phosphorus release from sediments: focused on phosphorus transfer and resupply across the sediment-water interface. Sci. Total Environ. 592, 662–673.
Zhang, X.H., Khan, A., Ducker, W.A., 2007. A nanoscale gas state. Phys. Rev. Lett. 98 (13), 136,101–136,104.
Zhang, H.G., Tao, L.Y., Lei, B., Grant, T., David, P.H., Pan, G., 2018. Combating hypoxia/anoxia at sediment-water interfaces: a preliminary study of oxygen nanobubble modified clay materials. Sci. Total Environ. 637, 550–560.